A Data-Driven and Personalized Stance Symmetry Controller for Robotic Ankle-Foot Prostheses: A Preliminary Investigation

Christopher Prasanna, Jonathan Realmuto, *Member, IEEE*, Anthony Anderson, Eric Rombokas, *Member, IEEE*, and Glenn Klute, *Member, IEEE*

***Abstract*— People with unilateral transtibial amputation generally exhibit asymmetric gait, likely due to inadequate prosthetic ankle function. This results in compensatory behavior, leading to long-term musculoskeletal impairments (e.g., osteoarthritis in the joints of the intact limb). Powered prostheses can better emulate biological ankles, however, control methods are over-reliant on non-disabled data, require extensive amounts of tuning by experts, and cannot adapt to each user's unique gait patterns. This work directly addresses all these limitations with a personalized and data-driven control strategy. Our controller uses a virtual setpoint trajectory within an impedance-inspired formula to adjust the dynamics of the robotic ankle-foot prosthesis as a function of stance phase. A single sensor measuring thigh motion is used to estimate the gait phase in real time. The virtual setpoint trajectory is modified via a data-driven iterative learning strategy aimed at optimizing ankle angle symmetry. The controller was experimentally evaluated on two people with transtibial amputation. The control scheme successfully increased ankle angle symmetry about the two limbs by 24.4% when compared to the passive condition. In addition, the symmetry controller significantly increased peak prosthetic ankle power output at push-off by 0.52 W/kg and significantly reduced biomechanical risk factors associated with osteoarthritis (i.e., knee and hip abduction moments) in the intact limb. This research demonstrates the benefits of personalized and data-driven symmetry controllers for robotic ankle-foot prostheses.**

***Index Terms*— Powered prosthetics, control systems, biomechanics, iterative learning control.**

Manuscript received 12 August 2022; revised 1 December 2022, 21 March 2023, 11 July 2023, and 22 September 2023; accepted 26 September 2023. Date of publication 13 October 2023; date of current version 20 October 2023. This work was supported by the United States Department of Veterans Affairs Rehabilitation Research and Development Service under Grant I01 RX003138, Grant I50 RX002357, and Grant IK6 RX002974. *(Corresponding author: Christopher Prasanna.)*

This work involved human subjects or animals in its research. Approval of all ethical and experimental procedures and protocols was granted by the Veterans Affairs Puget Sound Health Care System Institutional Review Board #2.

Christopher Prasanna, Anthony Anderson, and Glenn Klute are with the Center for Limb Loss and Mobility, Seattle, WA 98108 USA, and also with the Mechanical Engineering Department, University of Washington, Seattle, WA 98195 USA (e-mail: prasac@uw.edu; ajanders@uw.edu; gklute@uw.edu).

Jonathan Realmuto was with the Mechanical Engineering Department, University of Washington, Seattle, WA 98195 USA, and also with the Center for Limb Loss and Mobility, Seattle, WA 98108 USA. He is now with the Bionic Systems Laboratory, University of California at Riverside, Riverside, CA 92521 USA (e-mail: jrealmut@ucr.edu).

Eric Rombokas is with the Mechanical Engineering Department, and the Department of Electrical and Computer Engineering, University of Washington, Seattle, WA 98195 USA (e-mail: rombokas@uw.edu).

Digital Object Identifier 10.1109/TNSRE.2023.3322124

I. Introduction

TRADITIONALLY prescribed passive ankle-foot prostheses cannot completely replicate proper human ankle function since the passive components responsible for plantarflexion do not have the ability to generate mechanical power unlike human ankles [1]. Rather, passive ankle-foot prostheses can only store and return energy. As a result, individuals with transtibial amputation exhibit a number of neuromuscular adaptations to compensate for the loss of ankle function [2]. One of the most significant consequences of transtibial amputation is asymmetrical loading of the lower limbs during walking which can lead to a number of secondary conditions [3], including osteoarthritis (OA) in their intact knee and hip joints [4]. Studies have reported much larger peak knee abduction moments (KAM) and peak hip abduction moments (HAM), two well-studied risk factors of OA, in the intact limb of individuals with transtibial amputation when compared to their prosthesis side [5], [6]. Ankle-foot prostheses with improved push-off performance have shown to promote better walking patterns and reduce some of the risk factors associated with the degenerative diseases [7]. Therefore, there is a need to explore prosthesis designs that include and control actively-powered ankles, which have the potential to increase mobility and prevent secondary musculoskeletal conditions.

Powered ankle-foot prostheses (PAFPs) can potentially replicate human ankle behavior, however, current approaches are limited in their abilities to adapt and personalize to each individual. Many PAFPs utilize non-disabled gait data for determining controller parameters [8], [9]. However, metabolic rate, gait mechanics, and muscle activity can vary widely across non-disabled users as well as those with amputation [10]. Even when nominal non-disabled data are used, control parameter adjustments still need to be made, usually through trial and error [8], [9]. However, discovering the best user

parameters is time-consuming and challenging since tuning during clinical evaluations fails to demonstrate the same benefits as found in the laboratory [11]. Current PAFP devices are also limited in terms of how they can adapt to the user and their environment. These devices are typically restricted to changes in slopes [8] or speed [9].

Human-in-the-loop optimization (HILO) algorithms, where the prosthesis control commands are learned based on the human-robot response, could allow for long-term and more generalizable adaptations [12]. An important decision to make when designing a HILO algorithm is choosing the metric that the algorithm optimizes. Metabolic rate is a common optimization metric in HILO studies with lower limb exoskeletons [13]. However, a recent series of case studies were unsuccessful in extending HILO methods to powered prosthesis control for individuals with transtibial amputation when metabolic rate was used as an optimization target [14]. Though metabolic rate is important, other optimization targets may be more appropriate for people with transtibial amputation. The kinetic and kinematic gait deviations of this population have been studied extensively [15], [16], and are related to secondary musculoskeletal disease [4]. Therefore, HILO algorithms aimed at reducing gait asymmetries may be beneficial for PAFP controllers. One previous study explored transfemoral prosthesis controller personalization using HILO methods, however, the method used pre-collected gait data to fit parameters via linear regression [17]. This approach is limited, as it does not account for human adaptations to the control signal and the control law should adapt to these behaviors. Other studies have investigated HILO algorithms for personalized prosthesis control, but the methods have only been tested using prosthesis adapters with healthy control subjects thus far [18], [19].

The individual's ability to adapt and learn how to best use a powered prosthesis may play a key role in the outcomes. One study found that K4 ambulators could learn how to harness the power output of a powered prosthesis while K3 ambulators could not [11]. This could be an argument for personalized controllers since prosthesis assistance is learned based on observed human-robot responses, which may resolve the problems that K3 ambulators have in learning to use a powered prosthesis. Another study found that, for all ten individuals with unilateral transtibial amputation included in the experimental protocol, the best tested power setting for the BiOM prosthesis (BiOM T2 Ankle, BionX Medical Technologies Inc., Cambridge, MA) was consistently higher than the prosthetist-chosen setting [20]. This resulted in a statistically significant difference in metabolic cost between the best tested and prosthetist-chosen power settings. This finding further supports the argument for PAFP controllers that automatically personalize to the individual and do not rely on manual tuning.

One of the most popular PAFP control approach is to use a finite-state machine (FSM) [21]. Using sensor feedback to detect easily identifiable gait events (e.g., heel-strike, toe-off), these controllers decompose the periodic gait cycle into distinct phases. Each sub-phase (e.g., early stance, middle stance, and late stance) has its own controller, which typically is composed of a set of fixed parameters and a feedback control law (e.g., position control, impedance control). However, human locomotion is a continuous control process and it is difficult to emulate this natural behavior using distinct control laws. Additionally, as the number of sub-phases increases, the number of tunable control parameters may increase [22]. Current robotic prosthesis controllers are limited as they use a large amount of parameters that affect ankle torque output, even though manual tuning processes are only feasible with a handful of control parameters and predefined tasks. In addition, re-tuning sessions would be required as the user adapts their gait to the device over time. One study outlined an approach towards individual personalization and automatic control parameter tuning based on inverse reinforcement learning [23]. However, this method was only tested in simulation.

PAFPs have in general been shown to provide biomechanical advantages over passive devices, including increasing symmetry and ankle power production [24]. However, powered devices do not automatically confer these benefits, as they require careful tuning of the personalized controller parameters [21]. An outstanding challenge is to achieve these benefits automatically without expert tuning and it is this challenge that this work aims to address. The main contribution is a controller for a PAFP that optimizes ankle kinematic symmetry during stance phase using gait data from each individual. This method uses an offline iterative learning algorithm to optimize a virtual kinematic setpoint trajectory within an impedance control law. The control strategy directly addresses the limitations of using non-disabled gait data and the need for manual tuning by a clinical expert since the controller automatically learns and tunes the dynamics of the PAFP based on each individual. State estimation based on a biomechanical phase variable is also used, which enables the control law to be time-invariant and adapt to variations in the user's gait. Additionally, the controller acts continuously, eliminating the need to discretize the gait cycle and tune parameters to each sub-phase. The proposed controller was experimentally assessed with a prototype PAFP and two subjects with unilateral transtibial amputation. We hypothesized that the symmetry controller would (1) reduce ankle angle asymmetry, (2) reduce ankle power asymmetry, (3) reduce the intact peak KAM, and (4) reduce the intact peak HAM when compared to the prototype PAFP while in its passive mode (i.e., without active assistance from the electrical motor).

II. Methods

The real-time controller architecture is illustrated as a block diagram in Fig. 1. The offline symmetry learning method is displayed in Fig. 2. This research is an expansion of a previously-developed symmetry learning controller aimed at adjusting the PAFPs torque to match the achieved intact ankle torque using an adaptive gain iterative learning control strategy [25]. For this study, the learning approach was modified to target ankle angle symmetry rather than ankle torque symmetry because ankle kinematics are potentially easier to measure outside a laboratory setting, which is a future aim for this work. The contributions of the symmetry learning controller used in this study are the use of data-driven iterative learning

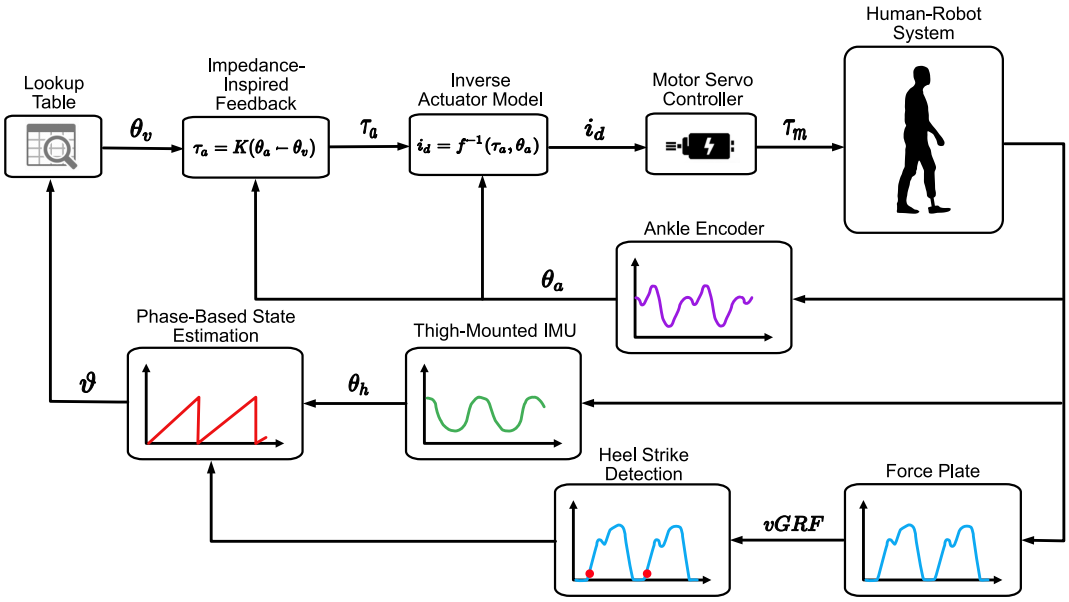

Fig. 1. Real-time PAFP control system architecture. Sensor measurements are fed to the control and state estimation algorithms. Global thigh angle estimations θ_h from the IMU signals and heel strike detections from the force plate signal *vGRF* are used to compute the phase-based state estimation. The phase variable value is then mapped to an instance along the gait cycle and its corresponding virtual setpoint signal value θ_v via a lookup table. The gait cycle information and the PAFP angle θ_a, measured from an encoder sensor, are then fed into the impedance-inspired feedback control law (Equation (1)). This formula outputs a desired active ankle torque τ_a which is fed into the inverse actuator model, which computes the motor current command i_d. Finally, this command is sent to the motor servo controller and the motor generates an assistive torque τ_m.

and phase-based state estimation to build a personalized and time-invariant impedance control law for the user.

A. Symmetry Control Strategy

1) Impedance-Inspired Feedback Control Law: This work proposes an impedance-inspired strategy for real-time feedback control of PAFPs. Impedance-based control was chosen since it is a flexible strategy based on the dynamic relationship between a change in the position of a joint and the corresponding torque response [26]. This allows the incorporation of both the motion and torque of the robotic joint into the control strategy at the same time. For this reason, impedance control is particularly well-suited for human-robot interaction and environmental interaction tasks. Additionally, prior research has shown that the human ankle displays time-varying mechanical impedance behavior [27], [28]. Thus, an impedance-based PAFP control law is biologically-inspired and has the potential to emulate human ankles. In order to adapt the control command signal to achieve the desired active assistance from the PAFP, an impedance-inspired formula was used as a feedback control law.

$$\tau_a(t) = K\left(\theta_a(t) - \theta_v(t)\right) \tag{1}$$

where K is the virtual ankle stiffness parameter, θ_a is the prosthetic ankle angle, and θ_v is a virtual setpoint signal. The desired active torque τ_a is then used within an inverse model of the prototype PAFP's actuator to produce a motor control command. Damping and inertia parameters were neglected from Equation (1) since stiffness dominates ankle behaviors within the sagittal plane [27], [28], and to reduce the overall controller complexity. The prosthetic ankle angle θ_a was measured in real time using an ankle-mounted 12-bit capacitive encoder (CUI Devices, AMT113S-V). The virtual setpoint signal θ_v is a learned trajectory that varies across the gait cycle and adjusts the quasi-stiffness behavior of the PAFP. In hardware, the virtual setpoint is discretized and encoded as a lookup table indexed by percent gait, which is estimated in real-time with the phase-based state estimator (§II-A.2).

In a previous study, the stiffness gain was defined as a time-varying parameter to estimate ankle impedance [28]. However, the impedance parameters were fit using data from ten young, active, and non-disabled subjects. It is well-understood that gait mechanics vary widely not only between those with and without amputations, but also within the general population [10]. Therefore, rather than relying on pre-determined stiffness trajectories, we instead chose to vary the virtual setpoint signal θ_v across the gait cycle and personalize its trajectory based on each user's unique biomechanics (i.e., iteratively adapt the trajectory based on ankle angle asymmetry measured by a motion capture system). Since θ_v is time-varying, any arbitrary quasi-stiffness (i.e., ankle torque-angle relationship) during walking can be achieved during walking. The virtual stiffness parameter K was held constant during this experiment. The value of the virtual stiffness parameter was determined based on pilot testing on a bench setup prior to human subject experiments. Quantifying the time-varying behavior of K and the prosthetic ankle's response to perturbations is outside the scope of this study. Finally, a static inverse actuator model, derived based on the PAFP's physical geometry, and the motor and drivetrain characteristics, was implemented to compute the motor current command given the desired active torque.

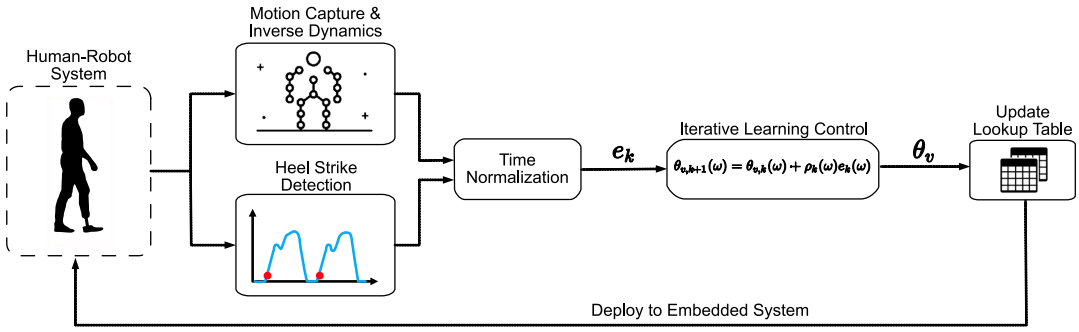

Fig. 2. Offline data processing and symmetry learning protocol. Motion capture marker and force plates data are processed offline after the completion of an experimental walking trial. Joint kinematics and kinetics are computed with inverse dynamics principles. In addition, heel strike events are computed from the force plate data and all biomechanical data are time-normalized using these instances. The time-normalized error signal e_k is then computed (Equation (5)) and fed into the iterative learning algorithm (Equation (3)). This algorithm outputs the updated virtual setpoint signal θ_V for the next walking trial. A pattern generator is then used to map the gait cycle to θ_V in the form of a lookup table. This new lookup table is then deployed to the PAFP's embedded system software for the next walking trial.

2) Phase-Based State Estimation: Since ankle impedance varies as a function of the gait cycle, the controller developed in this work included a phase variable calculator which acts as a time-invariant gait phase state estimator [29]. This technique required that the phase variable have a monotonic trajectory during steady state walking and be able to be computed from an unactuated state of the system. For this study, continuous phase-based control of the virtual setpoint trajectory is synchronized to the prosthesis-side thigh angle [30]. Using thigh angular position and its integral, the phase variable ϑ is computed in real time as

$$\begin{aligned} \vartheta[t] &= \frac{\text{atan2}(z\,Y[t],\ X[t]) - \vartheta^{+}}{\vartheta^{-} - \vartheta^{+}} \\ X[t] &= -\left(\theta_h[t] - \gamma\right) \\ Y[t] &= X[t]\,dt\ +\ Y[t-1] \end{aligned} \tag{2}$$

where θ_h represents the global thigh angle measured by a single thigh-mounted inertial measurement unit (IMU) sensor. Variables ϑ^{+} and ϑ^{-} normalize the phase variable trajectory across the gait cycle, i.e., $\vartheta \in [0, 1]$. The "+" and "–" superscripts indicate the phase variable starting value of the prosthetic-side stance period and ending value of the prosthetic-side swing period respectively. The phase variable is also clipped at an upper limit of 1 in order to avoid wraparound effects (i.e., discontinuities) caused by variations in thigh angle range of motion across gait cycles. Once the phase variable reaches a value of 1, it is held at this value until the next heel-strike (HS) event occurs which then resets the value to 0. The parameter z is a scale factor that increases the monotonicity of the phase variable while γ is a phase shift value that centers the thigh orbit around the origin of the phase portrait. These adaptive parameters are computed at each HS event based on the maximum and minimum values of X and Y across the previous gait cycle.

HS events were computed using vertical ground reaction force (vGRF) signals from an instrumented treadmill. The raw vGRF signal is digitally filtered using two digital low-pass Butterworth filters in series, each with a cutoff and sampling frequency of 50 and 500 Hz respectively. An estimate of the force rate of change is calculated as the difference between the first low-pass filter's output and the final filtered output. A HS event is determined by thresholding the vGRF signal and the force rate of change estimate. The vGRF signal during walking typically consists of two peaks: the impact peak during weight acceptance and active peak at push-off. In order to avoid false HS detection during the active peak, the vGRF signal was clipped at a magnitude lower than the magnitude of the two peaks. This resulted in a force rate of change signal with two distinct peaks which could be easily thresholded and used to estimate HS events.

3) Offline Data-Driven Iterative Learning: The goal of this study was to develop a controller that targets gait asymmetries. To achieve this, the controller must produce a control signal such that the dynamics of the PAFP match the dynamics of the biological ankle (i.e., intact ankle). The control signal (i.e., virtual setpoint trajectory), which modulates the active torque produced by the PAFP, is computed using Equation (1) where θ_v modifies the dynamical behavior of the PAFP over the gait cycle. An offline iterative learning control (ILC) method is used to update θ_v over learning iterations k in the frequency domain:

$$\theta_{v,k+1}(\omega) = \theta_{v,k}(\omega) + \rho_k(\omega)\, e_k(\omega) \tag{3}$$

where ρ_k is the adaptive learning gain, ω represents the frequency components of the discrete Fourier transform that form the signals, and e_k is the error signal. Note that the frequencies ω depend on the discretization of the time-normalization and the mean stride period T (i.e., mean time between HS events computed per walking trial), and are related by

$$\omega \in \left[0 \quad \omega_0 \quad 2\omega_0 \quad \ldots \quad \tfrac{N}{2}\omega_0\right], \quad \omega_0 = \frac{2\pi}{T} \tag{4}$$

where N is the number of points in the time-normalized gait cycle and ω_0 is the fundamental frequency of the mean stride period. Note that these frequencies are computed from the signals and not directly from cadence (e.g., stride period).

The error signal e_k in Equation (3) represents the ankle kinematic asymmetry, measured offline by an optical motion capture (MoCap) system, and is defined as the difference

between the time-normalized mean biological ankle angle signal $\bar{\theta}_{b,k}$ and the mean prosthetic ankle angle signal $\bar{\theta}_{p,k}$,

$$e_k(\omega) = \bar{\theta}_{b,k}(\omega) - \bar{\theta}_{p,k}(\omega) \tag{5}$$

In practice, the mean ankle kinematic signals at each iteration k are computed over an experimental 30-second walking trial by taking the mean value, at each discrete percent gait, over all full gait cycles. It was determined in preliminary experiments that 30-seconds of walking allowed for a sufficient number of steps to compute an average with high certainty, while not too long as to tire the participant.

Ideally, the ILC update law (Equation (3)) will be able to achieve convergence of the error signal by repeatedly executing the walking task. Convergence of the update law can be achieved at each frequency ω provided the reference signal (i.e., $\bar{\theta}_{b,k}$) is fixed. Since the control signal affects the biological kinematics θ_b, the reference signal can vary and thus, it may not be possible to guarantee convergence under these criterion. The reference signal $\bar{\theta}_{b,k}$ is driven by the human-response dynamics so the frequency-dependent learning gain ρ_k must be adapted such that the control signal remains bounded. The ILC update law in Equation (3) with a fixed learning gain could result in an unbounded actuator response, and poses a safety risk for the user.

To address this issue, an adaptive gain is applied to the ILC update law. The main purpose of the adaptive learning gain is to avoid potential divergence of the control input u which could risk the safety of the user. In previous studies, iteration conditions and convergence were investigated based on the selection of a frequency-dependent learning gain ρ_k for a human-robot collaborative task [31]. The results showed that the error achieved by the proposed adaptive learning gain was less than that of closed-loop tracking error. This adaptive learning gain monitors the output tracking error within the frequency domain across training iterations and reduces the magnitude of the gain if the tracking error increases. If the error e is decreasing at a specific frequency in training iteration k, then the learning gain at the specified frequency will not change from iteration $k-1$ to k. However, if the error increases at iteration step k for a specific frequency, then ρ at that frequency is scaled down until it converges to zero or the error decreases below the value at iteration step $k-1$. By monitoring the kinematic error signal e_k and adjusting the frequency-dependent learning gain ρ_k accordingly, the algorithm accounts for adaptations in the human response to the controller and the potential for divergence in the control signal is eliminated. Note that the frequency-dependent learning gain ρ_k adapts to changes in the error signal e_k offline to create a new virtual setpoint signal θ_v that is deployed to the PAFP system for the next walking trial. The adaptive learning gain is not used in the real-time PAFP control law and thus, does not adapt during stride.

B. Prototype PAFP Device

A prototype PAFP was used in this research and Fig. 3 shows the device and its subcomponents [25]. A cam-based spring acts across the ankle joint and provides a nonlinear elastic response which mimics the elastic response of a biological ankle [32]. The spring acts in parallel to the powered drivetrain which provides active torque and consists of a motorized link acting across the shank and ankle links. Including a passive element parallel to the actuator decreases the power requirements on the active component and also allows the device to function without assistance from the motor (i.e., acts as a passive device). The drivetrain consists of the following: a brushless DC motor, attached to a pin joint on the shank link, in series with a planetary gearhead, and followed by a linear ball screw attached to a pin joint on the ankle link that acts with a moment arm from the ankle joint. A compliant bumper, located between the ball screw nut and ball screw housing, protects the transmission from shocks, i.e., it engages near maximum plantarflexion. The mass of the prototype is 3.01 kg.

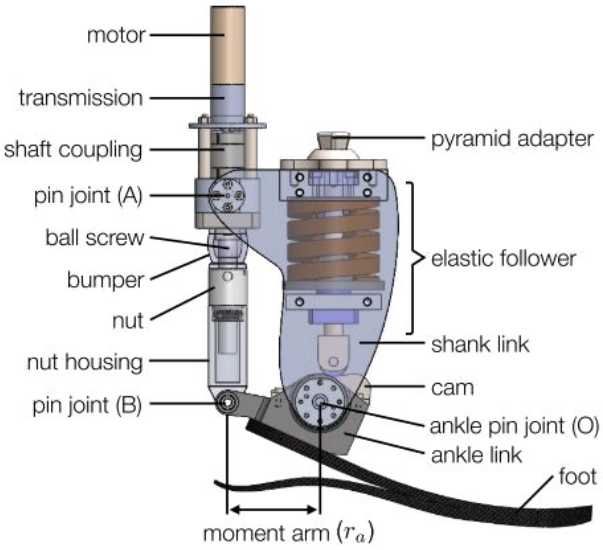

Fig. 3. Illustrative rendering of the prototype PAFP with major components labeled (note some components are transparent for ease in visualization).

TABLE I
SUBJECT-SPECIFIC PARAMETERS

	A01	A02
Age (years)	57	29
Height (cm)	178.5	164.5
Amputated Side	Right	Left
Mass with PAFP (kg)	89.9	84.1
Prescribed Prosthesis	Cheetah Xplore	Pro-Flex XC Torsion
Treadmill Speed (m/s)	1.0	0.7

C. Human Subject Experiments

The experimental setup consisted of an AMTI split-belt force-sensing treadmill, Vicon MoCap system with 16 Vantage V8 cameras, 63 reflective MoCap markers, and a human subject wearing the prototype PAFP connected to a custom embedded system and tethered power supply. Marker trajectories and ground reaction force (GRF) data were recorded at 120 Hz and 1200 Hz respectively. The raw data were filtered using a digital, fourth order, low-pass Butterworth

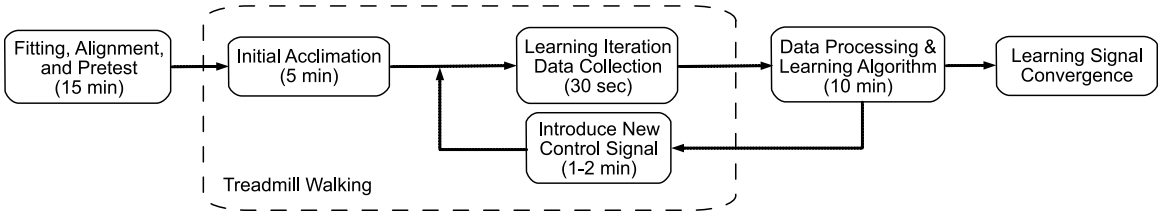

Fig. 4. Experimental protocol divided into three parts: setup (fitting, alignment, and choosing the bias current), walking trials (data collection), and offline computations (data processing and learning algorithm).

filter with cutoff frequencies of 25, 6, 50, and 50 Hz for kinetics, kinematics, GRF, and embedded system signals (i.e., motor currents and sensor signals) respectively. A custom 15-segment whole body model was created in Visual 3D and the markers on the prosthetic limb mirrored the markers on the intact limb. The model was adjusted by adding the difference between the masses of the prosthesis and the default foot segment to the prosthesis side shank mass, thereby manually compensating for the prosthesis mass within the model. The default segment masses are calculated as fractions of the total mass of the subject [33]. This method does not perfectly capture the inertial properties of the prosthesis. However, since the total prosthesis mass is concentrated along the shank and since inertial compensation model choice has been shown to have a small effect on the measured outcomes during stance phase [34], the error is likely small. Joint angles were calculated using inverse kinematics and joint moments were calculated using standard inverse dynamics [35] and normalized by the subject's body mass. Joint power contributions from deforming structures of the prosthesis were taken into account with the unified deformable segment method, enabling a better direct comparison between the variable prosthetic structural components and the anatomical properties of an intact ankle-foot system [36].

The prosthetic device was fit to the amputated limb of each subject by a certified prosthetist. The protocol was performed with two subjects with unilateral traumatic transtibial amputation who provided written informed consent to participate in the experimental protocol, approved by the Department of Veteran Affairs Institutional Review Board. Table I shows the subject-specific parameters. The subjects were healthy and active males (K3-level). This study can demonstrate the algorithm's performance, but future studies with more subjects will be needed to make broad conclusions about the controller's efficacy.

1) Protocol: Fig. 4 visualizes the experimental protocol and includes time estimates for each stage. At the start of the experiment, the prototype PAFP was fitted to the subject and they were asked to choose a bias current (i.e., offset in motor current that effectively shifts the equilibrium) for the device which felt comfortable during static standing. Due to the preload of the PAFP's nonlinear spring, which causes the prosthetic foot's resting position to be plantarflexed, this bias current was necessary in order to overcome the preload and adjust the neutral position of the prosthetic foot, which helps avoid toe drag during swing phases. Since the proposed control strategy is based on an iterative learning algorithm, there is no guarantee that the controller would learn to lift the toe high enough to clear the ground during swing for earlier learning iterations. This could risk the safety of the user and for this reason, we opted for the more stable and predictable approach of choosing a constant bias current before data collection and applying this current during swing phases. Choosing the bias current value took approximately 10 minutes. Afterwards, the subject walked on the treadmill at their self-selected speed for approximately 5 minutes and during this period, the bias current was then verified and adjusted further if necessary. Once the bias current had been determined, the experimental walking trials were collected, where each learning iteration k consisted of 30 seconds of steady state walking. Note that a control signal was not used during the first learning iteration ($k = 0$) and collected data from this trial represented the passive condition.

After each learning iteration k, the subject was allowed to rest while data were processed. HS events were identified post-hoc from the force plate data. All data were then time-normalized, via interpolation, to both 100% of gait and 100% of stance for statistical analysis. The mean time-normalized biological ankle angles and mean time-normalized prosthetic ankle angles were used to compute the error signal for the iterative learning algorithm. Since the PAFP is controlled via impedance control only during stance, the error signal was set to zero during 70-100% of the gait cycle. Using this technique, the swing phase errors did not directly influence the learned signal and the algorithm could better make improvements to the virtual trajectory during the phase where the controller is active. After each learning iteration, the new virtual setpoint trajectory was uploaded to the PAFP's embedded system. Prior to collecting the next trial, the subject first began walking while the PAFP was in its passive mode. Next, the new control signal was introduced over the course of $30-60$ seconds (i.e., by linearly scaling the signal). Once the subject had walked with the new control signal for 1-2 minutes, data for the next walking trial were collected. This process was repeated until the measured error signal could no longer be reduced, i.e., the learning signal converged.

2) Data Analysis: For this study, lower-limb joint kinematics and kinetics were processed in Visual 3D. The processed data were then exported to MATLAB for further analysis. For each gait variable, each individual gait cycle is assigned an asymmetry measurement (AM) by computing the average norm difference of the step of interest and the step of the contralateral limb occurring immediately before and after the step of interest. The AM for gait cycle s of some gait variable

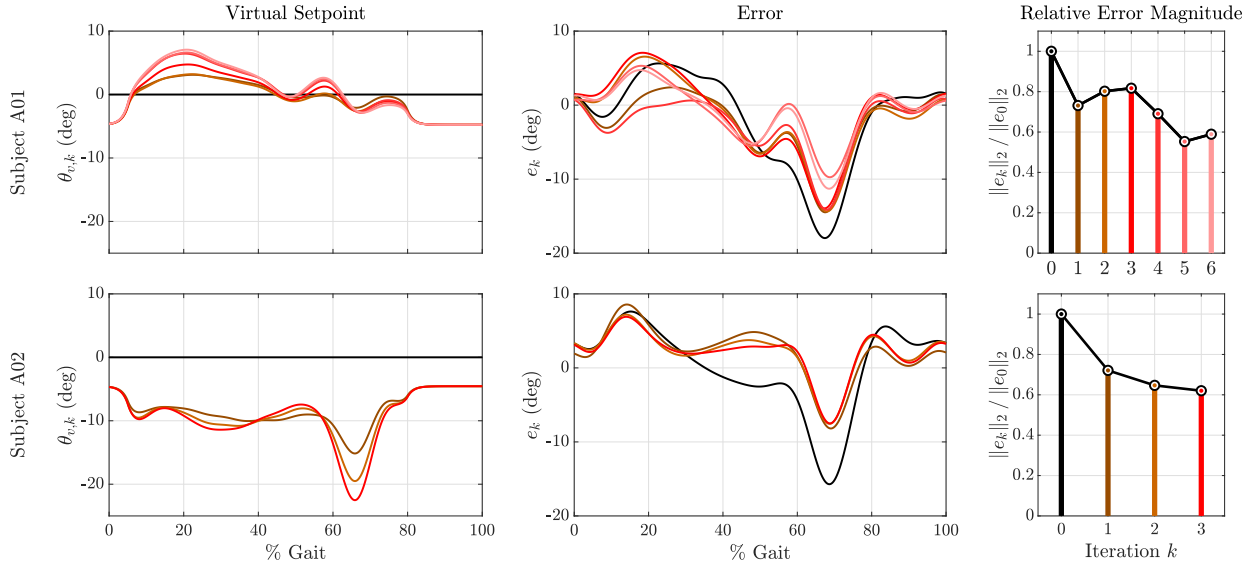

Fig. 5. Time domain evolution of the learned virtual (setpoint) trajectory $\theta_{V,k}$ (left column), iteration error e_k (center column), and relative error magnitude (right column) shown for each iteration k for both subject A01 (top row) and A02 (bottom row). Iteration $k = 0$ is black and subsequent iterations are increasingly lighter shades of red, as denoted by the X-axis label of the relative error magnitude plots (right column).

X can be computed as

$$AM(X_s) = \frac{1}{2}\|X_s - Y^-\|_2 + \frac{1}{2}\|X_s - Y^+\|_2 \qquad (6)$$

where X is the time series data of the gait variable of interest (e.g., prosthetic ankle angles) over gait cycle s and Y is the corresponding time series data of the contralateral limb (e.g., biological ankle angles). The "−" and "+" superscripts of variable Y indicate the vectors of data for the gait cycles before and after gait cycle s respectively. The 2-norm is defined as $\|\cdot\|_2 = \sqrt{(\cdot)^2}$. Note that this process is applied to each gait cycle within each walking trial and the result is a distribution of AMs for each trial. Therefore, it is possible to conduct statistical analysis comparing the AM distributions between experimental conditions (i.e., passive and active). However, due to the small sample size of this study ($n = 2$), the statistical results cannot be generalized to the entire target population. In an absolute best-case scenario (i.e., perfect symmetry), the AM value is equal to 0.

Hypothesis testing to detect pair-wise differences within each subject and overall differences for each outcome (e.g., peak PAFP angles, ankle angle asymmetry, peak PAFP powers, ankle power asymmetry, peak intact KAM, or peak intact HAM) and experimental condition (i.e., passive or active) were carried out using t-tests. The Benjamini-Hochberg correction was applied to the p-values to maintain a false discovery rate of 5%. No outliers were removed from the data using manual or systematic methods. The statistical significance criterion was $p < 0.05$. Results are presented as means for each outcome by condition and mean pairwise differences among conditions.

III. Results

This research demonstrates the potential for personalized PAFP control strategies. Hypothesis (1) was supported with significant reductions in ankle angle asymmetry when powered assistance was introduced. Hypothesis (2) was partially supported: powered assistance reduced asymmetries in ankle power for subject A02 but not for subject A01. Hypotheses (3) and (4) were supported with significant reductions in KAM and HAM on the intact limb when comparing the active condition to the passive condition.

A. Algorithm Performance

Fig. 5 shows the time domain signal traces at each learning iteration k. The learning algorithm produced bounded control signals for both subjects and all iterations k despite human adaptations. The differences in the virtual setpoint trajectory (left column of Fig. 5) across the two subjects is very apparent, which supports the concept that personalization is important for PAFP controllers. Also, each subject adapted to the controller very differently, indicating that each individual has their own ideal virtual setpoint trajectory. Subject A02's virtual setpoint trajectory noticeably changed only at the first learning iteration (i.e., $k = 1$) and changes in subsequent iterations were very small. Comparatively, subject A01 adapted much later into the experiment. Despite these variations in learning, the learning algorithm was able to avoid divergence in the control signal and reduce the error signal (center column of Fig. 5). The relative magnitude of each iteration error, calculated as $\|e_k\|_2 / \|e_0\|_2$, can be seen in the right column of Fig. 5. In subsequent analysis, the final iterations, $k = 6$ and $k = 3$ for A01 and A02 respectively, are used as the active condition trials.

B. Ankle Angle

Fig. 6 shows that the active assistance had an effect on the prosthesis-side ankle kinematics. There was no significant change in peak prosthetic plantarflexion angle or the peak intact plantarflexion between the passive and active conditions. The active condition significantly reduced the peak prosthetic dorsiflexion angle when compared to the passive condition ($p < 0.01$), however, this result may be skewed due to the

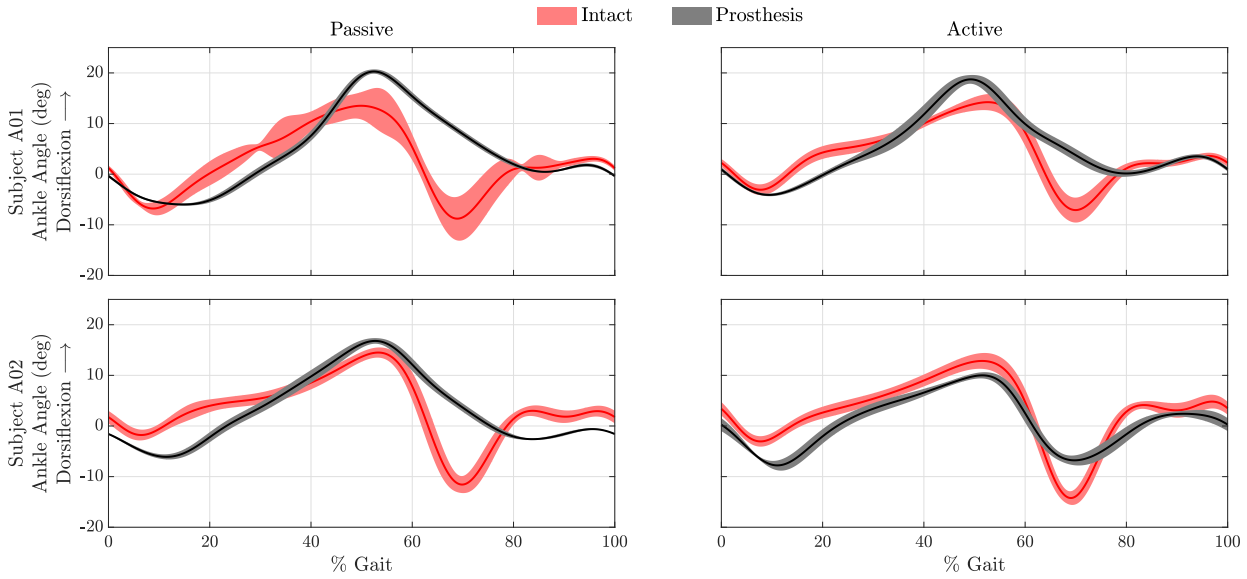

Fig. 6. Sagittal plane ankle angles for the two subjects during the two experimental conditions. Width of the traces represent ±1 standard deviation. Introducing active PAFP assistance resulted in a stabilization of the intact ankle (i.e., reduction in standard deviation) for subject A01 and a significant increase in prosthetic ankle plantarflexion during late stance for subject A02.

TABLE II
MEAN ANKLE ASYMMETRY OUTCOME MEASURES

	Passive	Active	Difference, p-value
Angle Asymmetry (rad)			
A01	0.89	0.60	-0.30, 1.04e-9
A02	0.83	0.71	-0.12, 1.23e-4
Combined	0.86	0.65	-0.22, 6.93e-13
Power Asymmetry (W/kg)			
A01	5.07	4.94	-0.13, 0.77
A02	3.33	2.53	-0.81, 7.99e-6
Combined	4.23	3.84	-0.39, 0.21

large reduction in prosthesis-side ankle dorsiflexion during subject A02's experiment (bottom row of Fig. 6).

Table II shows the ankle angle asymmetry measurement outcomes within each subject and overall. Ankle angle asymmetry was significantly different between the two conditions, with the active condition having lower ankle angle AM value (i.e., the active condition achieved better ankle angle symmetry). These results indicate that the symmetry controller successfully targeted and minimized ankle angle asymmetries.

C. Ankle Power

Peak positive and negative prosthetic ankle power outcomes were significantly altered across the two conditions (see Fig. 7 and 8). Peak positive prosthetic ankle power (i.e., ankle power generation) increased by 0.52 W/kg on average from the passive to active condition ($p < 0.01$). Negative prosthetic ankle power (i.e., ankle power dissipation) also significantly decreased by an average of 0.26 W/kg between these two conditions ($p < 0.01$). Peak PAFP power outcomes are shown in Table III and Fig. 8. Table II shows the ankle power asymmetry measurement outcomes within each subject and overall. Overall, the active condition did not significantly reduce ankle power asymmetry when compared to the passive condition ($p = 0.21$). We found that ankle power asymmetry significantly increased for subject A02 ($p < 0.01$), but not for subject A01 ($p = 0.77$).

D. Osteoarthritis Risk Factors in Intact Limb

Fig. 9 shows the peak intact-side KAM and HAM outcomes for the subjects and conditions. The active condition reduced the mean intact peak KAM from 0.48 Nm/kg to 0.43 Nm/kg, but did not reach the level of significance ($p = 0.14$). However, within each individual intact peak KAM was significantly reduced from 0.68 Nm/kg to 0.56 Nm/kg ($p < 0.01$) and from 0.29 Nm/kg to 0.26 ($p = 0.01$) for A01 and A02, respectively. Differences in peak HAM were also statistically significant across the two conditions. The active condition reduced the mean intact peak HAM from 0.54 Nm/kg to 0.48 Nm/kg ($p < 0.01$). Table III shows the peak intact KAM and HAM outcomes.

IV. DISCUSSION

There is currently no single standardized approach for reliably tuning powered lower-limb prostheses [21]. Our results indicate that the proposed symmetry controller, which combines an impedance type control law with a phase variable approach, achieves self-tuning behavior via iterative learning control. The controller demonstrated that directly targeting ankle kinematic symmetry through an impedance controller with a self-adjusting virtual trajectory is sufficient to realize many of the biomechanical advantages observed with expert tuning [24]. This work provides a new avenue for exploration to achieve advanced, capable, and personalized lower-limb prostheses.

A. Biomechanics

There was no significant change in peak prosthetic plantarflexion angle between the passive and active conditions but

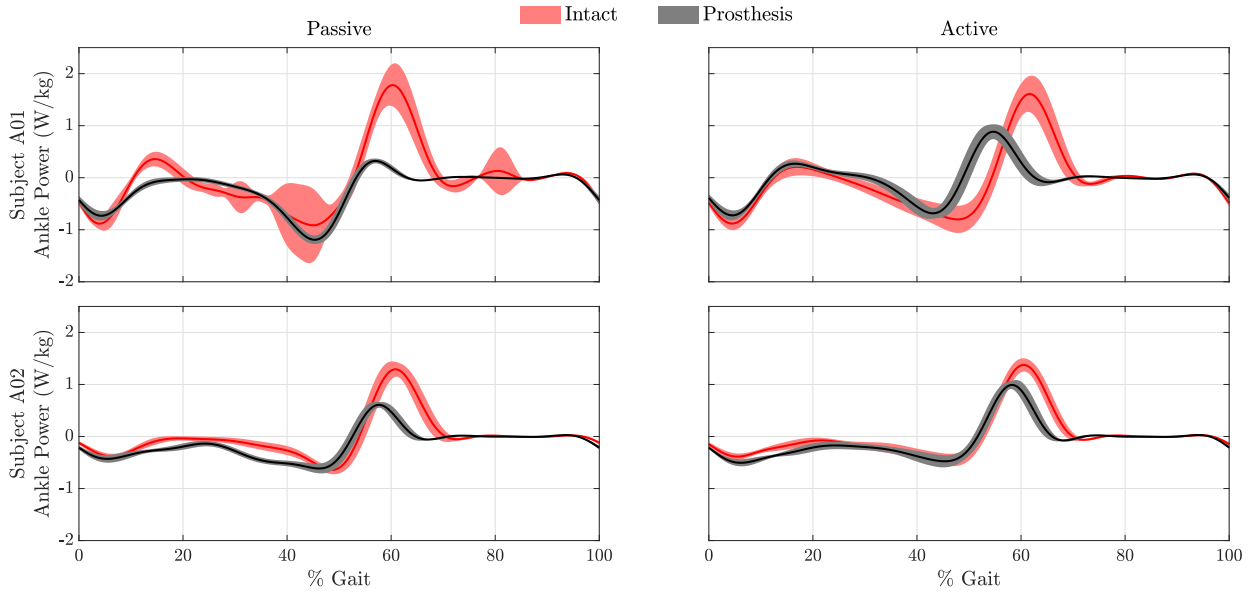

Fig. 7. Sagittal plane ankle power for the two subjects during the two experimental conditions. Ankle power is normalized by subject mass. Ankle power generation and dissipation are represented as positive and negative values respectively. Width of the traces represent ±1 standard deviation. For both subjects, introducing active PAFP assistance resulted in significantly greater peak positive prosthetic ankle power during late stance and reductions in negative prosthetic ankle power during mid-stance.

TABLE III
MEAN PEAK OUTCOME MEASURES

	Passive	Active	Difference, p-value
Positive PAFP Power (W/kg)			
A01	0.33	0.96	0.63, 2.25e-30
A02	0.65	1.03	0.40, 5.05e-22
Combined	0.48	0.99	0.52, 3.02e-31
Negative PAFP Power (W/kg)			
A01	1.21	0.78	-0.43, 6.14e-23
A02	0.64	0.55	-0.09, 7.65e-5
Combined	0.94	0.67	-0.26, 9.67e-7
Intact KAM (Nm/kg)			
A01	0.68	0.56	-0.12, 2.11e-14
A02	0.29	0.26	-0.03, 0.01
Combined	0.49	0.43	-0.06, 0.14
Intact HAM (Nm/kg)			
A01	0.58	0.52	-0.06, 8.68e-7
A02	0.50	0.44	-0.07, 4.92e-7
Combined	0.54	0.48	-0.06, 7.83e-7

this could be attributed to the different trends in each subject. Qualitatively, it is evident that the prosthetic ankle is actively plantarflexed near 70% gait during the active condition for subject A02. This was true for subject A01 as well, albeit, to a much lesser degree. The increase in plantarflexion is notable and suggests the advantages of PAFPs since common passive prostheses are not able to actively promote plantarflexion.

The active condition resulted in modified biological ankle angle trajectories for both subjects when compared to the passive condition (Fig. 6), although our statistical tests did not reach significance. This finding supports the notion that the behavior of the limbs are coupled, therefore, modifying and improving the behavior of the prosthetic limb can benefit the biomechanics of the intact limb [2], [15], [16]. Even though the prosthesis ankle kinematics look similar between conditions for subject A01, the active assistance appeared to decrease the variance of their biological ankle kinematics. This can be observed by the decrease in standard deviation (red shaded regions in Fig. 6) from the passive condition to the active condition. This observation further illustrates how improving the functionality of the prosthetic limb can benefit the other limb as well [2], [15], [16]. Furthermore, the reduction in peak prosthetic dorsiflexion angle as a result of active assistance suggests that the algorithm learned to support the users throughout mid-stance.

The results of this experiment also indicate that the kinematic symmetry learning controller improves prosthetic ankle power outcomes (i.e., increases positive power and decreases negative power). Interestingly, peak prosthetic ankle power at late stance significantly increased even though the learning algorithm was never explicitly programmed to prescribe an increase in ankle power. Yet, this behavior emerges from the symmetry controller, which is very desirable since ankle plantar flexors produce over 80% of the mechanical power generated during walking [1]. However, many clinically-prescribed prostheses fail to offer proper ankle push off power. This further supports the notion that powered ankle-foot prostheses can better emulate the dynamics of a human ankle. In this case, the learning algorithm is effectively improving PAFP power completely on its own using only ankle angles as a metric.

The symmetry controller also adapted to significantly reduce peak KAM and HAM in the intact limb without explicit programming. The reduction in these two well-studied risk factors associated with OA illustrate the clinical benefits of PAFPs and the proposed control method. All lower-limb joint biomechanics are affected by PAFP control as evident by this research, even when only targeting ankle angle asymmetries.

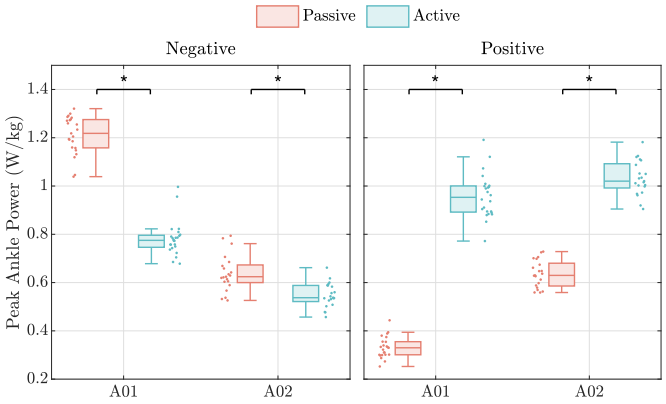

Fig. 8. Peak negative (dissipative) and positive (generative) prosthetic ankle power outcomes for each subject and the two experimental conditions. Each marker represents the outcome for a particular gait cycle and the asterisks indicate statistical significance ($p < 0.01$). The active condition resulted in significantly lower peak negative prosthetic ankle power outcomes and significantly greater peak positive prosthetic ankle power outcomes for both subjects.

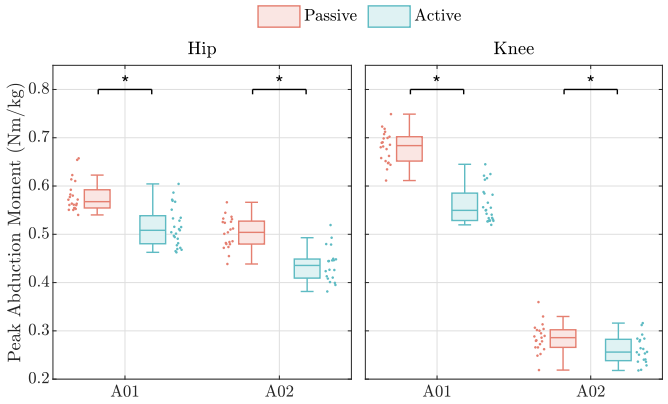

Fig. 9. Peak intact-side knee and hip abduction moment outcomes for each subject and the two experimental conditions. Each marker represents the outcome for a particular gait cycle and the asterisks indicate statistical significance ($p < 0.01$). The active condition resulted in a significant decrease in peak intact-side knee and hip abduction moments for both subjects.

This suggests that lower-limb joints are strongly coupled and therefore, improving prosthetic ankle function via powered assistance can reduce compensations at the hip and knee.

B. Limitations and Future Work

The biological ankle position adapted significantly during learning, particularly for subject A01's experiment. This is evident by the smaller standard deviation of the ankle angle results for the active condition compared to the passive condition. However, since the passive condition was the first condition tested, it is possible that the participant grew accustomed to the device over time and this could explain the lower variance in the active condition's ankle angle results. Conversely, it is possible that not enough time was given to rest between walking trials. Subject A01 experienced some swelling and pain in the residual limb due to the demands of the experimental protocol, which could have affected the results at later learning iterations. Additionally, it is possible that not enough time was given to acclimate to the learned signal at each iteration before collecting data. Furthermore, the algorithm is sensitive to the frequency-dependent error. As the error grows in certain frequencies, on the next iteration, those frequencies will become less sensitive to error and therefore, stop changing. If, on the other hand, the error continues to decrease at a certain frequency, learning will continue in those frequencies. It is likely the error for subject A02 increased for many (but not all) of the frequencies at each iteration but decreased for subject A01.

While the current experimental protocol shows that symmetry ILC has a lot of potential to improve walking mechanics, future experimental protocols can be improved. The underlying ILC algorithm [32] is limited in the number of possible iterations since the frequency-dependent learning gain is reduced aggressively if an increase in error is observed. The conservative nature of the algorithm is intended to prevent divergence of the control signal, however, future implementations with some relaxations may provide enhanced learning, including the possibility of more learning iterations. A long-term protocol, where more learning iterations are collected over the course of multiple sessions, would allow more time for the user to acclimate to the controller. This would also assist in convergence of the learned signal.

A limitation of our phased-based state estimation is the requirement that the phase variable, computed from the prosthesis-side thigh angle, have a monotonic trajectory. While this requirement was not violated during our preliminary work, simulations, and experiments involving steady-state walking on a treadmill, other situations where the user's gait is not consistent may require a different approach. The use of rigid body biomechanics models to calculate ankle angles is also limiting [36]. Future studies should also include experiments with more than two subjects in order to analyze more meaningful and generalizable biomechanical trends across conditions. The statistical results from this study only apply to the sample population and cannot be generalized to the larger population with transtibial amputation. In addition, adding new experimental conditions (e.g., load carriage, stair walking, ramp walking, etc.) may demonstrate the benefits of the symmetry controller to a greater degree.

The proposed method still requires that the subject complete an experimental protocol in the laboratory. However, by eliminating the need for iterative, multi-parameter tuning, there is much less lab time effort when compared to the process of tuning state-based controllers. The proposed symmetry learning control strategy avoids key limitations that could exclude PAFPs from future clinical application including the need for subject-specific tuning, non-disabled trajectory data, and allows both the human and controller to jointly adapt.

A limitation of the proposed learning approach is the use of inverse kinematics for estimating ankle angle asymmetry. This is restrictive since learning can only be conducted in a gait laboratory setting. While it is possible to estimate the ankle angles in real-time with external sensors, we opted to use MoCap because of its proven reliability, accuracy, ease of use, and direct availability to the research team. Our goal was to demonstrate the underlying algorithm and therefore we sought to minimize confounding challenges when possible.

Future embodiments would fully embed the required sensors for online implementations. Improvements to the inverse dynamics model can be made (e.g., accounting for the elastic behavior of the foot keel, using the PAFP mass as a model parameter, and setting a custom ankle joint center for the PAFP) and this is an ongoing research topic in the field of biomechanics [36]. Furthermore, the current learning protocols are run offline since MoCap data needs to be manually labeled and processed. Future development could include the use of a high-fidelity model (e.g., neural network) or sensors (e.g., wearables) to enable online HILO methods (e.g., [37]). This way, study subjects could use the PAFP controller outside the laboratory and we can assess its benefits in this setting. Furthermore, long-term learning protocols could be conducted with continuous learning and without any reliance on optical MoCap, which could provide insights into long-term co-adaptations between users and PAFPs.

In this study, despite the experimental protocol only including steady state walking, co-adaptations were observed as evidenced by the intact ankle kinematics adapting as the control signal was iteratively modified (results not shown). Future implementations should consider co-adaptations, for example, to increase or decrease the learning time scale (i.e., time between updates) and allow the human user to fully adapt to the control signal before the next learning iteration. One possibility is to monitor the rate of change of the intact ankle angle adaptations and scale the timing of the controller updates accordingly. This could further decrease the required time to complete the experiment (if the human adapts quickly) and prevent a situation where the learned signals diverge (if the human adapts slowing), e.g., applying a new learning update before the human fully adapts could produce a divergent control signal. Another improvement to the control system would be to include a phase-varying stiffness parameter. In the current control scheme, only the virtual setpoint trajectory is varied and therefore, only the quasi-stiffness characteristics of the PAFP can be modified [38]. A phase-varying stiffness parameter could be used to render biomimetic ankle impedance properties while the learned virtual setpoint trajectory used in this study would adapt to personalize PAFP assistance to each user. However, ankle impedance during walking for people with unilateral transtibial amputation needs to be determined before implementing a phase-varying stiffness parameter into the impedance control law. In addition, a more complex impedance model that includes dampening is worth exploring in the future. Another avenue is addressing the ideal virtual trajectory, which is unknown and most likely personalized for each individual. Impedance system identification methods that include estimation of a virtual trajectory could provide estimates on the mean and variance, subsequently bootstrapping our algorithm with an initial guess.

V. Conclusion

This work proposes a symmetry control strategy for robotic ankle-foot prostheses. The novelty of this methodology is the personalization of an impedance-inspired feedback control law based on each individual's unique gait data. This data is used to adjust the dynamics of the PAFP to match the dynamics of the individual's biological ankle. By automatically tuning the control trajectory, this approach does not rely on non-disabled gait data, which is a common limitation found in state-of-the-art PAFP controllers. In addition, this method does not require precise tuning of a large amount of parameters. An experimental study ($n = 2$) was conducted to test if the learning algorithm and control strategy would reduce ankle asymmetries and loading factors on the intact limb associated with OA. The results indicate that the proposed control method was able to significantly improve ankle angle and ankle power symmetry when compared to using the prototype PAFP with no active assistance. Additionally, the proposed approach significantly reduced intact-side KAM and HAM when compared to the passive condition. Therefore, this research demonstrates that designing controllers to improve symmetry about the ankle joints can result in improvements at other joints of the lower limb (e.g., intact ankle, knee, and hip), which motivates further investigation toward personalized PAFP symmetry controllers.

References

[1] D. A. Winter, "Energy generation and absorption at the ankle and knee during fast, natural, and slow cadences," *Clin. Orthopaedics Rel. Res.*, vol. 175, pp. 147–154, May 1983.

[2] P. G. Adamczyk and A. D. Kuo, "Mechanisms of gait asymmetry due to push-off deficiency in unilateral amputees," *IEEE Trans. Neural Syst. Rehabil. Eng.*, vol. 23, no. 5, pp. 776–785, Sep. 2015.

[3] D. C. Morgenroth, A. C. Gellhorn, and P. Suri, "Osteoarthritis in the disabled population: A mechanical perspective," *PM&R*, vol. 4, no. 5, pp. S20–S27, May 2012.

[4] R. Gailey, "Review of secondary physical conditions associated with lower-limb amputation and long-term prosthesis use," *J. Rehabil. Res. Develop.*, vol. 45, no. 1, pp. 15–30, Dec. 2008.

[5] T. D. Royer and C. A. Wasilewski, "Hip and knee frontal plane moments in persons with unilateral, trans-tibial amputation," *Gait Posture*, vol. 23, no. 3, pp. 303–306, Apr. 2006.

[6] C. H. Lloyd, S. J. Stanhope, I. S. Davis, and T. D. Royer, "Strength asymmetry and osteoarthritis risk factors in unilateral trans-tibial, amputee gait," *Gait Posture*, vol. 32, no. 3, pp. 296–300, Jul. 2010.

[7] E. R. Esposito and J. M. Wilken, "Biomechanical risk factors for knee osteoarthritis when using passive and powered ankle–foot prostheses," *Clin. Biomech.*, vol. 29, no. 10, pp. 1186–1192, Dec. 2014.

[8] M. F. Eilenberg, H. Geyer, and H. Herr, "Control of a powered Ankle–Foot prosthesis based on a neuromuscular model," *IEEE Trans. Neural Syst. Rehabil. Eng.*, vol. 18, no. 2, pp. 164–173, Apr. 2010.

[9] A. H. Shultz, B. E. Lawson, and M. Goldfarb, "Variable cadence walking and ground adaptive standing with a powered ankle prosthesis," *IEEE Trans. Neural Syst. Rehabil. Eng.*, vol. 24, no. 4, pp. 495–505, Apr. 2016.

[10] D. A. Winter, "Kinematic and kinetic patterns in human gait: Variability and compensating effects," *Hum. Movement Sci.*, vol. 3, nos. 1–2, pp. 51–76, Mar. 1984.

[11] E. S. Gardinier, B. M. Kelly, J. Wensman, and D. H. Gates, "A controlled clinical trial of a clinically-tuned powered ankle prosthesis in people with transtibial amputation," *Clin. Rehabil.*, vol. 32, no. 3, pp. 319–329, Mar. 2018.

[12] D. Gopinath, S. Jain, and B. D. Argall, "Human-in-the-loop optimization of shared autonomy in assistive robotics," *IEEE Robot. Autom. Lett.*, vol. 2, no. 1, pp. 247–254, Jan. 2017.

[13] J. Zhang et al., "Human-in-the-loop optimization of exoskeleton assistance during walking," *Science*, vol. 356, no. 6344, pp. 1280–1284, Jun. 2017.

[14] C. G. Welker, A. S. Voloshina, V. L. Chiu, and S. H. Collins, "Shortcomings of human-in-the-loop optimization of an ankle-foot prosthesis emulator: A case series," *Roy. Soc. Open Sci.*, vol. 8, no. 5, May 2021, Art. no. 202020.

[15] D. A. Winter and S. E. Sienko, "Biomechanics of below-knee amputee gait," *J. Biomech.*, vol. 21, no. 5, pp. 361–367, Jan. 1988.

[16] H. Bateni and S. J. Olney, "Kinematic and kinetic variations of below-knee amputee gait," *JPO J. Prosthetics Orthotics*, vol. 14, no. 1, pp. 2–10, Mar. 2002.

[17] N. A. Kumar, S. Patrick, W. Hong, and P. Hur, "Control framework for sloped walking with a powered transfemoral prosthesis," *Frontiers Neurorobot.*, vol. 15, p. 182, Jan. 2022.

[18] M. Jacobson et al., "Foot contact forces can be used to personalize a wearable robot during human walking," *Sci. Rep.*, vol. 12, no. 1, pp. 1–12, Jun. 2022.

[19] T.-C. Wen, M. Jacobson, X. Zhou, H.-J. Chung, and M. Kim, "The personalization of stiffness for an ankle-foot prosthesis emulator using human-in-the-loop optimization," in *Proc. IEEE/RSJ Int. Conf. Intell. Robots Syst. (IROS)*, Oct. 2020, pp. 3431–3436.

[20] K. A. Ingraham, H. Choi, E. S. Gardinier, C. D. Remy, and D. H. Gates, "Choosing appropriate prosthetic ankle work to reduce the metabolic cost of individuals with transtibial amputation," *Sci. Rep.*, vol. 8, no. 1, Oct. 2018, Art. no. 15303.

[21] M. R. Tucker et al., "Control strategies for active lower extremity prosthetics and orthotics: A review," *J. NeuroEng. Rehabil.*, vol. 12, no. 1, pp. 1–30, 2015.

[22] B. E. Lawson, A. H. Shultz, and M. Goldfarb, "Evaluation of a coordinated control system for a pair of powered transfemoral prostheses," in *Proc. IEEE Int. Conf. Robot. Autom.*, May 2013, pp. 3888–3893.

[23] W. Liu, R. Wu, J. Si, and H. Huang, "A new robotic knee impedance control parameter optimization method facilitated by inverse reinforcement learning," *IEEE Robot. Autom. Lett.*, vol. 7, no. 4, pp. 10882–10889, Oct. 2022.

[24] E. Lathouwers et al., "Therapeutic benefits of lower limb prostheses: A systematic review," *J. NeuroEng. Rehabil.*, vol. 20, no. 1, pp. 1–27, 2023.

[25] J. Realmuto, G. Klute, and S. Devasia, "Preliminary investigation of symmetry learning control for powered ankle-foot prostheses," in *Proc. Wearable Robot. Assoc. Conf. (WearRAcon)*, Mar. 2019, pp. 40–45.

[26] N. Hogan and S. Buerger, "Impedance and interaction control," in *Robotics and Automation Handbook*, 1st ed. Boca Raton, FL, USA: CRC Press, 2004, p. 24.

[27] H. Lee and N. Hogan, "Time-varying ankle mechanical impedance during human locomotion," *IEEE Trans. Neural Syst. Rehabil. Eng.*, vol. 23, no. 5, pp. 755–764, Sep. 2015.

[28] E. J. Rouse, L. J. Hargrove, E. J. Perreault, and T. A. Kuiken, "Estimation of human ankle impedance during the stance phase of walking," *IEEE Trans. Neural Syst. Rehabil. Eng.*, vol. 22, no. 4, pp. 870–878, Jul. 2014.

[29] D. Quintero, D. J. Villarreal, D. J. Lambert, S. Kapp, and R. D. Gregg, "Continuous-phase control of a powered Knee–Ankle prosthesis: Amputee experiments across speeds and inclines," *IEEE Trans. Robot.*, vol. 34, no. 3, pp. 686–701, Jun. 2018.

[30] D. J. Villarreal and R. D. Gregg, "Unified phase variables of relative degree two for human locomotion," in *Proc. 38th Annu. Int. Conf. IEEE Eng. Med. Biol. Soc. (EMBC)*, Aug. 2016, pp. 6262–6267.

[31] J. Realmuto, R. B. Warrier, and S. Devasia, "Iterative learning control for human-robot collaborative output tracking," in *Proc. 12th IEEE/ASME Int. Conf. Mech. Embedded Syst. Appl. (MESA)*, Aug. 2016, pp. 1–6.

[32] J. Realmuto, G. Klute, and S. Devasia, "Nonlinear passive cam-based springs for powered ankle prostheses," *J. Med. Devices*, vol. 9, no. 1, Mar. 2015, Art. no. 011007.

[33] W. T. Dempster, "Space requirements of the seated operator," Aero Med. Lab., Wright Air Develop. Center, Air Res. Develop. Command, United States Air Force, Wright-Patterson Air Force Base, OH, USA, WADC Tech. Rep. 55-159, 1955.

[34] J. D. Smith, A. E. Ferris, G. D. Heise, R. N. Hinrichs, and P. E. Martin, "Oscillation and reaction board techniques for estimating inertial properties of a below-knee prosthesis," *J. Visualized Experiments*, no. 87, May 2014, Art. no. e50977.

[35] D. Winter, *The Biomechanics Motor Control Human Gait: Normal, Elderly Pathological*, 2nd ed. Waterloo, Oo, Canada: Univ. Waterloo Press, 1991.

[36] K. E. Zelik and E. C. Honert, "Ankle and foot power in gait analysis: Implications for science, technology and clinical assessment," *J. Biomech.*, vol. 75, pp. 1–12, Jun. 2018.

[37] J. R. Koller, D. H. Gates, D. P. Ferris, and C. D. Remy, "Body-in-the-Loop optimization of assistive robotic devices: A validation study," in *Robotics: Science and Systems*. Ann Arbor, Mi, USA: Univ. Michigan, 2016.

[38] E. J. Rouse, R. D. Gregg, L. J. Hargrove, and J. W. Sensinger, "The difference between stiffness and quasi-stiffness in the context of biomechanical modeling," *IEEE Trans. Biomed. Eng.*, vol. 60, no. 2, pp. 562–568, Feb. 2013.